

# Learning Wheelchair Tennis Navigation from Broadcast Videos with Domain Knowledge Transfer and Diffusion Motion Planning

Zixuan Wu<sup>1†</sup>, Zulfiqar Zaidi<sup>1†</sup>, Adithya Patil<sup>1†</sup>, Qingyu Xiao<sup>1</sup> and Matthew Gombolay<sup>1</sup>

**Abstract**—In this paper, we propose a novel and generalizable zero-shot knowledge transfer framework that distills expert sports navigation strategies from web videos into robotic systems with adversarial constraints and out-of-distribution image trajectories. Our pipeline enables diffusion-based imitation learning by reconstructing the full 3D task space from multiple partial views, warping it into 2D image space, closing the planning loop within this 2D space, and transfer constrained motion of interest back to task space. Additionally, we demonstrate that the learned policy can serve as a local planner in conjunction with position control. We apply this framework in the wheelchair tennis navigation problem to guide the wheelchair into the ball-hitting region. Our pipeline achieves a navigation success rate of 97.67% in reaching real-world recorded tennis ball trajectories with a physical robot wheelchair, and achieve a success rate of 68.49% in a real-world, real-time experiment on a full-sized tennis court.

## I. INTRODUCTION

Leveraging web videos of expert performance offers a promising way to train robots, particularly in agile robotics and sports, where gathering expert demonstrations—such as in wheelchair tennis—is extremely challenging. Numerous human-designed mechanical prototypes have demonstrated capabilities in various sports, including table tennis [1]–[3], badminton [4], [5], tennis [6]–[9], and soccer [10]. Although humans and robots share similar decision loops (e.g., perception, planning, and control) [11], research in robotic sports has yet to explore learning agile and dynamic behaviors from web expert videos, a gap we aim to address. Prior work in robotic sports has primarily focused on ball motion prediction [12], [13] and motion planning [14], [15] using techniques ranging from sophisticated hybrid ball dynamics models [14], [16] to simplified approaches like virtual hitting points [17] or linear collision models [18]. Reinforcement learning (RL) [19] and imitation learning (IL) [20] have also shown promise in sports robotics [21], [22], but RL requires extensive training in simulated environments and IL depends on costly expert demonstrations.

Images and videos have become popular sources of demonstrations for IL [23], [24]. Although advanced generative models can reason within image space, their imitation policies typically rely on static objects without autonomous dynamics (e.g., manipulated objects in pick-and-place tasks) [23], [25], [26]. Additionally, these methods often require costly human demonstrations captured with depth or multi-view cameras. To overcome the limited availability of learning sources, research has suggested using web videos from

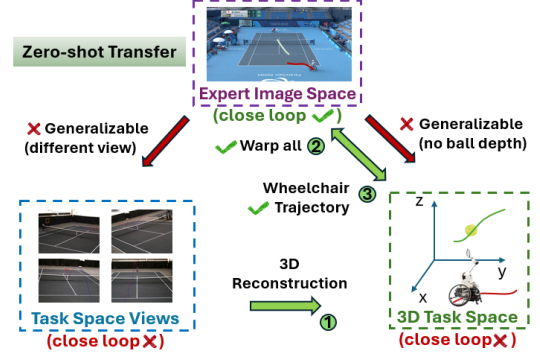


Fig. 1: Motivation: Learning from web videos. We propose a three-step approach: 1) reconstruct full 3D motion in the task space (ball-wheelchair), 2) project all motions into the 2D expert image space to apply the imitation policy, and 3) transfer planar wheelchair motion back to the 3D task space.

monocular cameras as a vast, accessible resource. However, these videos are often noisy and incomplete, necessitating information extraction to obtain valuable data. Notably, Zhang et al. [27] demonstrated that a simulated agent could learn to play tennis using data collected from broadcast videos using a combination of IL and RL, but this approach was only applied in simulation.

Our work differs from previous video learning approaches [23], [24], [28], [29] in two ways. First, we utilize an autonomous wheelchair robot that operates in a challenging, adversarial setting, with less than two seconds to intercept an incoming tennis ball moving under its own dynamics. This requires our IL model to respond to dynamic ball trajectories in real-time, rather than relying on static text commands or navigation goals. Second, the disparity in perspectives between web videos and our real-world setting makes 2D-to-2D generalization impossible, and the lack of tennis ball depth information in monocular video streams prevents 2D-to-3D scene reconstruction. To address this out-of-distribution (OOD) challenge, we reconstruct the 3D scene from multiple partial camera views in our task space, project the objects into the expert’s 2D image space, run the imitation policy there, and transfer the resulting 2D robot motion back to the 3D task space (see Figure 1).

Our contributions are as follows:

- To best of our knowledge, we are the first to tackle the web video learning problem in agile navigation under adversarial settings with OOD task space. We propose a novel zero-shot knowledge transferring framework with a diffusion motion planner that can also be generalized

<sup>†</sup> Equal contribution

<sup>1</sup> Authors are affiliated with the Georgia Institute of Technology, Atlanta, GA 30332 USA. Corresponding author: Zixuan Wu (zwx380@gatech.edu)

to other 2D mobile robot navigation problems.

- We incorporate mean-shift matchplay identification and audio segmentation model into our online broadcast wheelchair tennis data extraction pipeline, which is able to handle raw, unprocessed broadcast footage and help efficiently produce training-ready data.
- We design a real-time feedback planning-control system, including a PD controller guided by our IL policy, and demonstrate zero-shot transfer to a real robot on a real tennis court. We show our method outperforms baselines in multi-level ablation studies.

## II. RELATED WORK

### A. Robotics in Athletics

Robotic platforms in athletics can be classified by maneuverability into fixed, locally moving, and globally moving systems. Fixed platforms, like stationary manipulators for table tennis [1] and badminton [4], are limited to returning balls within a small range. Locally moving platforms, enhanced with gantry rails [5], [7], [30], offer more mobility, but remain restricted in reach and are often costly [7].

This paper focuses on a global court navigation system for a wheelchair tennis robot [6], using a mobile electric wheelchair base. While similar to previous systems [8], [31] due to its mobile base, our platform differs in that the wheelchair robot meets Paralympic tennis standards.

### B. Vision-based Planning and Control

Visual information has long been used in robot planning and control, starting with visual servo techniques [32], [33] and visual teach-and-repeat methods. Recent works use visual prompts [34], affordances [25], or vision-based rewards [26] to inform motion planning via machine learning on videos. For example, RT-Trajectory [34] generates actions based on static sketched, demonstrated, or language-guided trajectories. In contrast, our approach generates trajectories using a diffusion model that responds to dynamic tennis ball trajectories. Although reward functions can be learned from videos to score optimal trajectories [26], these methods rely on separate visual model predictive control (VMPC) for trajectory sampling, limiting their ability to perform zero-shot motion planning. Bahl et al. [25] address this by generating trajectories using a Transformer with learned visual affordances, but their approach operates slowly in static environments without feedback, making it unsuitable for our fast-paced, adversarial game setting.

Few studies shift the decision or planning loop into the image space, as most prior work generates [35], [36] or optimizes [37] trajectories in 3D task space before projecting them into the image space. In contrast, we aim to learn a navigation policy directly from web videos, eliminating the need for hand-crafted motion planning, costly wheelchair player demonstrations or environment interactions. While prior work has used video features for reward shaping [38], [39] or goal conditions [25] in RL, these methods still depend on human demonstrations and environment interactions.

### C. Motion Planning with Imitation Learning

IL based motion planning originated with behavior cloning (BC) and its application in autonomous driving, using images and laser inputs to predict direction [40]. The issue of compounding errors in BC over time [41] was addressed by the Dataset Aggregation (DAgger) algorithm [42], which requires interaction with expert policies and the environment, contrary to the zero-shot learning approach we envision. The pseudo-action labeling approach, such as BCO [28], learns a dynamic model for mobile robots during exploration to estimate inter-frame actions in observations and construct experience tuples for BC. Although this algorithm has been applied to visual navigation problems by associating YouTube video frames with actions and rewards in Q-learning [29], it requires ego-centric observations, pre-defined navigation goals, and real-world exploration by the robot, which are impractical in our context.

Diffusion probabilistic models are generative models that denoise Gaussian noise into in-distribution samples under certain constraints [43]–[46]. To tackle the state drift problem in Markov-based BC, researchers have proposed diffusion-based long-horizon path planning, demonstrating both global effectiveness and local consistency [47]–[49]. However, these global plans are generated only once with initial constraints, lacking in-task feedback and real-time performance guarantees. Recently, diffusion [23] and transformer-based trackers [20], [24] have been proposed to mitigate compounding errors by integrating sequential position control or guiding policy learning. However, they still rely on static objects or text inputs and sometimes require action labels [20].

## III. METHODOLOGY

In this work, we develop a pipeline that extracts data from wheelchair tennis broadcast videos, learns a policy on the extracted data in image space, and transfers it to a real-world wheelchair robot. Our dataset and implementation scenarios span two distinct domains: the training data is derived from monocular 2D broadcast video footage of the 2020 Paralympics tennis game, while the algorithm must be applied in a real 3D tennis court environment with different views from external wall cameras (see Figure 1-2). This discrepancy poses significant challenges for knowledge transfer. Additionally, we aim to achieve zero-shot sim-to-real transfer without any interactive fine-tuning.

Our method addresses these challenges through four components: (1) data extraction from broadcast videos (Sec. III-A), (2) a knowledge transfer framework (Sec. III-B), (3) imitation policy learning (Sec. III-C), and (4) real-time feedback control for execution on the robot (Sec. III-D).

### A. Data Extraction from Broadcast Videos

The goal of this phase is to extract player movement data from broadcast wheelchair tennis videos. We used footage from the singles matches from the Tokyo 2020 Paralympic Games. The extraction process involves six steps (Fig. 4): (1) Using a mean-shift model to filter non-matchplay segments, (2) Training a neural network to detect ball hit audio, (3)

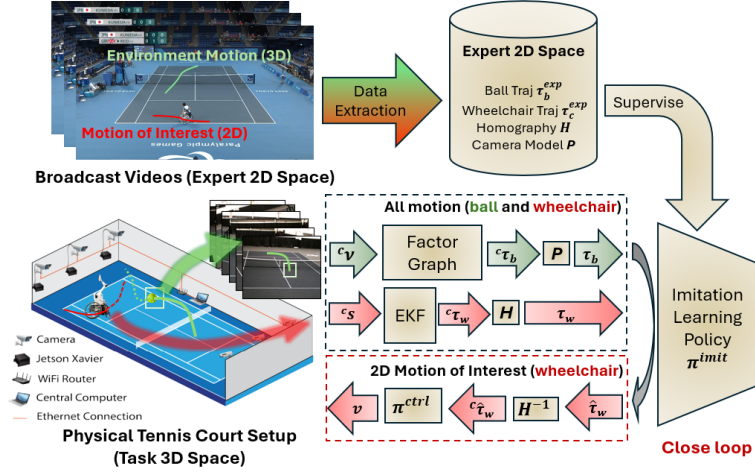


Fig. 2: Overview of our knowledge transferring framework: The wheelchair motion is the motion of interest (MOI, indicated by red) since we need to control it in our task space. The ball motion is the environment motion (Env-M, indicated by green) on which the wheelchair should condition. The knowledge transfer is valid with the only assumption that MOI is 2D motion and Env-M can be 3D.

Obtaining court homography, (4) Tracking the tennis ball, (5) Locating the player on the nearside of the court, and (6) Aggregating the data for training output.

First, we train two models: one to filter non-matchplay footage and another to detect ball hits using match audio. The matchplay filtering model applies Mean Shift clustering with a flat kernel to preprocessed video frames—resized, Gaussian filtered, converted to grayscale, and intensity rescaled—to retain only matchplay portions. The algorithm updates each data point  $x_i$  (a frame) using  $x_i \leftarrow \frac{\sum_j K(x_j - x_i)x_j}{\sum_j K(x_j - x_i)}$ , where  $K$  is a flat kernel. The hit detection model utilizes a fully connected neural network with three layers (sizes 256, 128, and 2) on audio features extracted via Mel-frequency cepstral coefficients (MFCCs), chromagrams, and mel-spectrograms [50]. The network is trained by minimizing the cross-entropy loss  $L = -[y \log(\hat{y}) + (1 - y) \log(1 - \hat{y})]$  (where  $y$  is a binary indicator for hit) on manually labeled audio clips of hits and randomly selected non-hit clips. Prior methods [51], [52] lacked this automatic matchplay and ball hit detection capability.

In the third and fourth steps, we track the tennis ball using TrackNet [51], [52] and generate the homography matrix for court identification using the methods from [53], [54]. The homography matrix translates pixel positions from the 2D image plane to 3D court coordinates, accounting for perspective distortion. The relationship between image coordinates  $(u, v)$  and court coordinates  $(x, y)$  is defined as:  $\begin{bmatrix} u' & v' & w \end{bmatrix}^\top = \mathbf{H} \begin{bmatrix} x & y & 1 \end{bmatrix}^\top$  where  $\mathbf{H}$  is the homography matrix. Unlike prior methods [53], [54], we recalculate the matrix only when camera motion is detected, improving efficiency. In the fifth step, we use an open-source object detection model [55] to detect the player on near-side of the court every ten frames, with background subtraction and

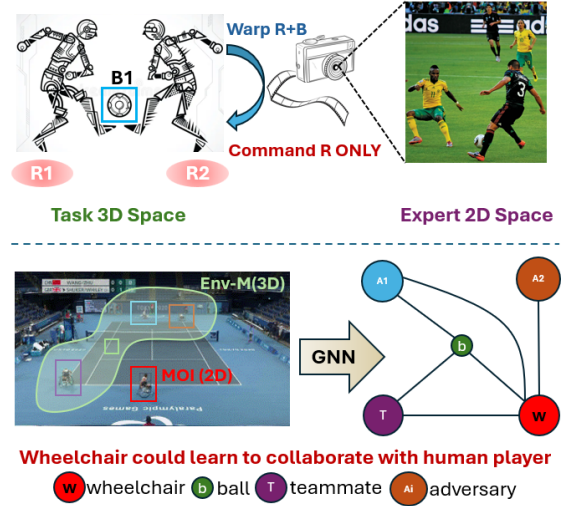


Fig. 3: Our framework can generalize to different scenarios, multi-agent settings and various imitation policies. The upper plot shows robot soccer [10] where  $R_i$  are 2D robots and  $B_1$  is the soccer ball. The lower plot depicts collaborative navigation learning with graph neural networks (GNNs).

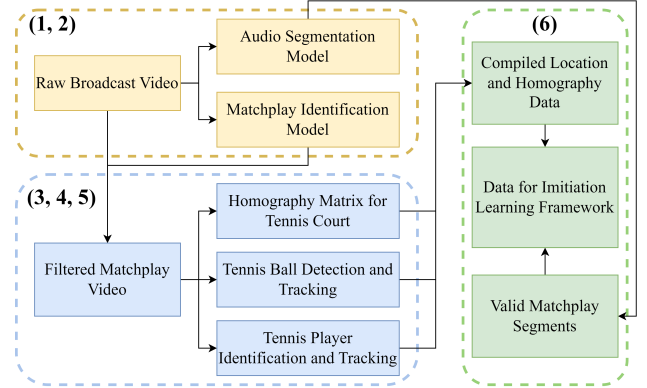


Fig. 4: Various steps involved in creating the dataset from broadcast footage of Paralympic 2020 games.

contour detection combined with an extended Kalman Filter for tracking in between frames. The homography matrix is then applied to determine the player’s position on the court relative to the baseline.

The final step involves segmenting the data into matchplay episodes (910 in total). Each episode begins when the far-side player hits the ball and ends when the near-side player returns it, as detected using the ball hit model. Afterwards, we can examine individual episodes and optionally discard invalid ones (we call it semi-automatic mode if we have this manual check). The data includes the 2D ball trajectory, the near-side player’s trajectory in 2D image and 3D task space, along with the homography matrix for each frame.

#### B. Knowledge Transferring Framework Design

We utilize our web-sourced Paralympics’ wheelchair tennis videos (expert 2D image space) as our training dataset (Sec. III-A), with the objective of executing the learned policy on a robot in a physical tennis court (3D task space).

---

**Algorithm 1: Knowledge Transferring Framework**

---

**Data:**  $\mathcal{D}$  (expert videos),  ${}^c\mathcal{T}_b, {}^c\mathcal{T}_w$  (tennis ball and wheelchair trajectory in task space),  ${}^cX_w$  (wheelchair position on the court in task space),  ${}^c\mathcal{V}$  (multiple partial views from wall cameras on the court in task space),  ${}^c\mathcal{S}$  (wheelchair on board sensors)

$\triangleleft$  Extract ball and wheelchair trajectories  $\mathcal{T}_b^{\text{exp}}, \mathcal{T}_w^{\text{exp}}$ , camera model  $P$  and homography  $H$  from expert video

- 1  $\mathcal{T}_b^{\text{exp}}, \mathcal{T}_w^{\text{exp}}, P, H = \text{VideoTracker}(\mathcal{D})$ ;
- $\triangleleft$  Learn the imitation policy  $\pi^{\text{imit}}$
- 2  $\pi^{\text{imit}} = \text{TrainPolicy}(\mathcal{T}_b^{\text{exp}}, \mathcal{T}_w^{\text{exp}})$ ;
- $\triangleleft$  Reconstruct 3D trajectories with factor graph and EKF
- 3  ${}^c\mathcal{T}_b = \text{FactorGraph}({}^c\mathcal{V}), {}^c\mathcal{T}_w = \text{EKF}({}^c\mathcal{S})$ ;
- $\triangleleft$  Warp trajectories  ${}^c\mathcal{T}_b, {}^c\mathcal{T}_w$  into the expert image space
- 4  $\mathcal{T}_b = P({}^c\mathcal{T}_b), \mathcal{T}_w = H({}^c\mathcal{T}_w)$ ;
- $\triangleleft$  Apply the imitation policy on the expert image space
- 5  $\hat{\mathcal{T}}_w = \pi^{\text{imit}}(\mathcal{T}_b, \mathcal{T}_w)$ ;
- $\triangleleft$  Convert desired wheelchair trajectory to task space  ${}^c\hat{\mathcal{T}}_w$
- 6  ${}^c\hat{\mathcal{T}}_w = H^{-1}(\hat{\mathcal{T}}_w)$ ;
- $\triangleleft$  Execute the control policy  $\pi^{\text{ctrl}}$  on the robot
- 7  $v = \pi^{\text{ctrl}}({}^cX_w, {}^c\hat{\mathcal{T}}_w)$

---

Given that our expert video data comes from a single camera angle without depth (similar to TV broadcasts) different from task space view configurations, it is neither feasible to fully reconstruct expert data in the 3D task space nor perform direct 2D-2D knowledge transfer. To address this, we design an algorithm (Algorithm 1) that bypasses the need for full 3D scene reconstruction by leveraging motion and visual geometry constraints through the following steps: (1) extract training data from broadcast videos (line 1); (2) train the imitation policy in the 2D image space using the extracted data (line 2); (3) in a real-world court setup, reconstruct the ball and wheelchair trajectories in 3D task space using multiple partial views from wall cameras and onboard wheelchair sensors, leveraging a factor graph [56] and Extended Kalman Filter (EKF) [57] (line 3); (4) project the 3D locations of the ball and wheelchair into the 2D image space using the camera model (line 4); (5) run the imitation policy to generate the desired wheelchair trajectory in the 2D image space (line 5); (6) transform the desired wheelchair trajectory from the 2D image space to the 3D task space using the inverse homography matrix (line 6 - possible since the wheelchair always remains on the ground plane); and (7) execute the trajectory on the wheelchair in real-time using a feedback controller (line 7). The process is visualized in Fig. 2, and our knowledge transferring framework can be generalized to other 2D constrained motion settings, multi-agent collaborations and imitation policy structures (Fig. 3).

### C. Imitation Policy Learning

Our imitation policy operates in the image space, where noise and uncertainty affect web video data and task space trajectory estimation. To address this, we employ a diffusion

---

**Algorithm 2: Diffusion Training and Sampling**

---

**Data:**  $\mathcal{T}_w, \mathcal{T}_b$  (wheelchair and ball image trajectories)

$\triangleleft$  Extract the trajectory pieces  $\mathcal{T}_b^{\text{sub}}, \mathcal{T}_w^{\text{sub}}$

- 1  $\mathcal{T}_b^{\text{sub}}, \mathcal{T}_w^{\text{sub}} = \text{Segment}(\mathcal{T}_b, \mathcal{T}_w)$ ;
- 2 **while** Training iteration **do**
  - $\triangleleft$  Draw training trajectory  $\tau$ , diffusion timestep  $i$ , and random noise  $\epsilon$
  - 3  $\tau_0, m \sim \mathcal{T}_b^{\text{sub}}; i \sim \mathcal{U}(1, T), \epsilon \sim \mathcal{N}(0, I)$ ;
  - $\triangleleft$  Apply the scheduled noise to the drawn trajectory
  - 4  $\tau_i \leftarrow \sqrt{\alpha_i}\tau_0 + \sqrt{1 - \alpha_i}\epsilon$ ;
  - $\triangleleft$  Compute MSE Loss and update model  $s_\theta$
  - 5  $\mathcal{L}(\theta) = \|\epsilon - s_\theta(\tau_i, i, m)\|_2^2$ ;  $\theta = \theta + \alpha \nabla_\theta \mathcal{L}(\theta)$ ;
- 6 **end**
- 7  $\tau^T \sim \mathcal{N}(0, I)$ ;  $\triangleleft$  Sample from Gaussian noise
- 8 **for all**  $i$  from  $T$  to 1 **do**
  - $\triangleleft$  Denoise the trajectory for one step
  - 9  $(\mu^i, \Sigma^i) \leftarrow s_\theta(\tau^i), \Sigma_\theta(\tau^i)\tau^{i-1} \sim \mathcal{N}(\mu^i, \Sigma^i)$ ;
  - $\triangleleft$  Sample from denoised distribution, apply constraints
  - 10  $\tau^{i-1} \sim \mathcal{N}(\mu^i, \Sigma^i)$ ;  $\tau^{i-1} \leftarrow \mathcal{C}(\tau^{i-1})$
- 11 **end**

---

policy that recovers in-distribution trajectories from noisy inputs, with prior work showing strong generalizability with corrupted data [58] and image-space operations [20] (see Algorithm 2). First, we segment the wheelchair and ball trajectories to an appropriate length (line 1). A batch of random trajectories  $\tau_0$  is drawn from the dataset (line 3) and Gaussian noise is applied using a cosine schedule (line 4). The training step involves calculating the MSE between the applied noise and the noise predicted by our model  $s_\theta$  and updating the model via gradient descent (line 5). During sampling, we apply our denoising model  $s_\theta$  to random Gaussian noise and enforce constraints to ensure that the diffusion trajectory starts at the current location (line 10).

Additionally, we train other baseline policies using our framework: the Action Chunking with Transformers (ACT) model [24], a fully connected regression neural network (FCR), and an autoencoder combined with a fully connected regression neural network (AE+FCR). In the AE+FCR model, the autoencoder encodes the prior ball trajectory, and the fully connected network predicts the commanded trajectory based on the wheelchair’s current position and the encoded prior ball trajectory.

### D. Real-time Reactive Feedback Control

Once the trajectory is provided by the imitation policy in the image space, it is converted to task space using inverse homography projection and executed on the robot in real-time using a proportional-derivative (PD) position controller. Assuming the wheelchair has a heading angle  $\theta$ , the origin of the control coordinate system is defined as the current position of the wheelchair. The relative coordinates of the desired position are  $[x, y]$ . Our PD controller is defined as:

$$v = k_{1p}(x \cos \theta + y \sin \theta) + k_{1d}\dot{x} \quad (1)$$

$$\omega = k_{2p}(\arctan 2(y, x) - \theta) + k_{2d}\dot{\theta} \quad (2)$$



The commanded driving speed  $v$  is proportional to the Cartesian error along the wheelchair’s heading direction, while the angular velocity  $\omega$  is proportional to the angular error. The derivative terms  $\dot{x}$  and  $\dot{\theta}$  stabilize the control. Together,  $v$  and  $\omega$  form the commanded twist, which is converted to left and right wheel velocities by a differential drive controller and executed on the robot.

#### IV. EXPERIMENTAL RESULTS AND DISCUSSION

In this section, we first evaluate the efficiency of our data extraction pipeline (Sec. IV-A). Next, we assess the performance of our knowledge transferring framework with diffusion imitation policy and compare it against various baselines by measuring the predictions against the expert ground-truth data (Sec. IV-B). Subsequently, we evaluate the effectiveness of our method in intercepting real-world ball trajectories in a hybrid testing (Sec. IV-C) and real-time real-court experiments (Sec. IV-D).

##### A. Data Extraction Pipeline

Previous tennis video tracking packages [51], [52] focus solely on trajectory and court line extraction. In contrast, our data extraction pipeline automatically isolates gameplay sections and filters out irrelevant content, such as crowd shots and player close-ups (see Fig. 5), removing approximately 54% of frames from a match video and generating episodes for downstream learning tasks. Furthermore, perform player detection (using an object detection model) every 10 frames, reducing reliance on image recognition models to just 10% of the time, further optimizing efficiency.



Fig. 5: The pipeline filters out rest and replay frames (top) while extracting relevant gameplay data (bottom).

##### B. Trajectory Prediction from Imitation Learning

In this section, we benchmark various policies trained using our framework by comparing the predicted trajectories of each method against the ground truth wheelchair trajectories extracted from broadcast videos. The methods include the diffusion policy (ours), Action Chunking Transformer (ACT), fully connected network regression (FCR), and auto-encoder-based policy (AE+FCR).

We test all these methods on two datasets: one collected by our full automatic data extraction pipeline (see Sec. III-A) and a smaller, semi-automatic dataset where we manually discard outlier trajectories. Therefore, the semi-automatic dataset is smaller but of higher quality. For both datasets, we measure the following metrics:

- **RMSE:** Average root mean square error between the predicted and the ground truth trajectory (meters).

- **Dynamic Time Warping (DTW) distance:** The cumulative DTW distance between predicted and the ground truth trajectory and trajectory (meters).
- **Iterative Closest Point (ICP) distance:** The mean distance between the predicted and the ground truth trajectory after aligning them using ICP (meters).
- **Jerk:** Root mean square jerk the robot would experience if following the predicted trajectories ( $m/s^3$ ).

For all metrics, a lower score indicates better performance, as shown in Table I. The “conditioning mode” specifies how the model was conditioned: “Pre 2D” refers to conditioning on prior ball observations in image space, while “Post 2D” refers to conditioning on future ball observations. Additionally, the “action mode” specifies whether the policy outputs results in image space ( $I_{space}$ ), which are then converted to Cartesian task space, or directly in task space ( $T_{space}$ ).

We observe from Table I that conditioning on the future ball trajectory yields better predictions across most metrics compared to conditioning on the prior observed trajectory, due to the additional future information guiding the wheelchair’s movement. The diffusion model outperforms ACT, FCR, and AE+FCR in RMSE by 20.6%, 5.4%, and 47.8%, and in jerk by 71.84%, 69.58%, and 70.46%, respectively. Figure 6 shows the diffusion trajectories alongside the ground truth (GT) trajectories. Both quantitative and visual results demonstrate that the diffusion model can generate smoother trajectories that closely follow expert paths with small diffusion steps (10 steps) and inference time ( $\approx 0.1s$ ), which reveals the possibility to learn the motion planning and close the decision loop in the image space.

We conduct an additional ablation where the diffusion policy is conditioned on the predicted 2D ball trajectory but outputs the wheelchair trajectory directly in Cartesian space. This performs significantly worse than outputting in 2D space, validating the advantage of keeping the whole imitation process in image space. Additionally, we find that the trajectory prediction results from the automatic dataset are generally slightly worse than those from the semi-automatic datasets, which meets our expectations since the semi-automatic dataset has higher quality. Consequently, in subsequent evaluations, we opted to use diffusion policies with action predictions in image space trained from semi-automatic dataset.

##### C. Hardware-in-Loop Task Space Hybrid Test

We conducted a series of hybrid tests, which combine real-world and simulated components, using a physical wheelchair robot and replayed real tennis ball trajectories collected on a tennis court. Balls were launched to various parts of the court (see Fig. 8 for trajectory distribution). These recorded trajectories were replayed, and the response of the physical wheelchair robot was recorded.

Since no expert ground truth trajectory is available in the task space, we use success rate as the evaluation metric. Success is defined as the wheelchair getting close enough for interception (within 1.4 meters of the ball) before it bounces three times (as wheelchair tennis permits up to two

TABLE I: Benchmarking results for imitation learning models across various metrics

Method	Condition	Action	Semi-Automatic				Automatic			
			RMSE	DTW	ICP	Jerk	RMSE	DTW	ICP	Jerk
Diffusion (ours)	Pre 2D	$I_{space}$	0.321	6.891	0.206	1.951	0.359	7.581	0.259	4.760
Diffusion (ours)	Post 2D	$I_{space}$	<b>0.277</b>	<b>5.880</b>	<b>0.167</b>	<b>1.150</b>	0.346	7.586	<b>0.218</b>	4.360
ACT	Pre 2D	$I_{space}$	0.372	8.400	0.212	5.879	0.403	9.090	0.266	6.037
ACT	Post 2D	$I_{space}$	0.381	8.640	0.226	5.274	0.387	8.810	0.242	4.976
FCR	Pre 2D	$I_{space}$	0.345	7.520	0.216	5.596	<b>0.321</b>	<b>7.250</b>	0.236	1.024
FCR	Post 2D	$I_{space}$	0.287	6.180	0.183	4.598	0.399	9.270	0.243	<b>0.876</b>
AE+FCR	Pre 2D	$I_{space}$	0.573	12.28	0.375	5.248	0.435	9.402	0.298	8.506
Diffusion	Post 2D	$T_{space}$	0.716	15.854	0.552	4.870	0.747	16.42	0.586	5.867

TABLE II: Comparison of success rate (SR) of different methods in hybrid(H) and real-court(R) settings.

Method	Conditioning	SR (H)	SR (R)
Diffusion (ours)	Post 2D	<b>97.67%</b>	<b>68.49%</b>
FCR	Post 2D	<b>97.67%</b>	55.58%
TEB	Post 3D	37.21%	35.36%



Fig. 7: Tennis robot responds to a ball launch over time. The ball is highlighted in the images.

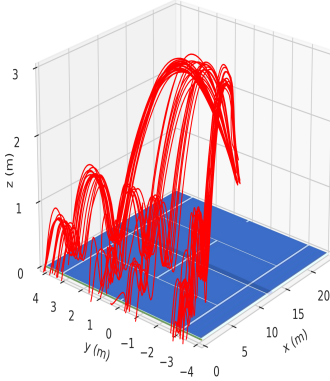


Fig. 8: Ball trajectory distribution of collected dataset.

bounces). The results obtained are documented in Table II. To compare performance, we also evaluated the best-performing imitation policies against a non-learning-based strategy from [6], referred to as the TEB baseline. The TEB baseline continuously monitors the ball's predicted trajectory and identifies positions within the robot's geometric hitting constraints. The Timed Elastic Band planner [59], a standard 2D navigation planner in ROS, estimates which point the robot can reach fastest, and then navigates to it. Both diffusion and FCR imitation policies trained with our framework outperform the TEB baseline, achieving a high success rate of 97.67%.

#### D. Real-time Experiment on a Tennis Court

In this section, we present the results of our real-world, real-time experiment as an end-to-end evaluation using a robot on a full-sized tennis court with real tennis balls.

**Setup:** Our system includes a wheelchair robot equipped with LiDAR, IMU, and wheel encoders, using an EKF for localization [57]. This localization informs our policies and provides feedback to the Proportional-Derivative (PD) controller. Six cameras are placed around the court for tennis ball tracking, each connected to a Jetson Xavier for ball detection. Detections are sent via ethernet to an offboard computer, which uses a factor graph-based approach to predict the ball trajectory [56] as input to the imitation policy. The data flow between components is shown in Fig. 9.

The results are tabulated in Table II, where it shows the

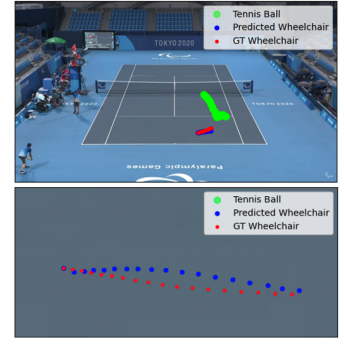


Fig. 6: Diffusion Trajectory

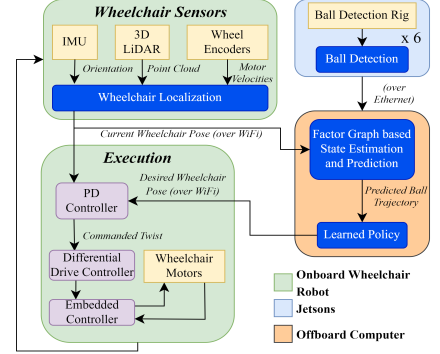


Fig. 9: Data flow between different components of the system for real-time experiment on a full-sized tennis court.

diffusion policy with our learning framework outperforms the FCR and TEB by 12.91% and 33.13% in the real-world setting. We provide snapshots of the policy execution on the physical robot in real-time with a real ball on a full-sized tennis court as illustrated in Fig. 7. The performance gap between experiments using real-time trajectories and those playing back recorded trajectories indicates that on-the-fly trajectory estimation in the large court has negative effects on the agile navigation task due to observation uncertainty and communication delays. The result shows diffusion-based motion planner is more robust to such system disturbance.

#### V. CONCLUSION AND FUTURE WORK

We propose a zero-shot knowledge transferring framework that constructs a full 3D scene in task space, warp the scene into monocular 2D image space to extract expert knowledge, and transfers the motion of interest back to task space with visual geometry constraints. By learning from web videos, our approach eliminates the need for static-goal, ego-centric, multi-view, or physical demonstrations, outperforming baselines in both simulation and real-world experiments. This work opens new avenues for research in human-robot collaboration (Fig. 3) and manipulation strategies that enable not only intercepting the ball but also successfully returning it. To further enhance real-world performance, future work could focus on accelerating diffusion sampling using Denoising Diffusion Implicit Models (DDIM) [60] and incorporating constraints that improve trajectory smoothness.

## APPENDIX I WHEELCHAIR ROBOT DETAILS

The wheelchair used is a Top End Pro Tennis wheelchair, motorized for autonomous control. A chain-drive system delivers power from the motors to the wheels. Each wheel is powered by a motor coupled to a 1:10 ratio speed-reducer planetary gearbox. The gearbox output shaft is connected to the wheel through a chain and sprocket system, providing an additional 1:2 speed reduction, resulting in a total reduction of 1:20. At maximum motor speed, the wheelchair can achieve linear velocities of up to 10 m/s and an in-place angular yaw velocity of up to 20 rad/s. Localization is achieved using wheel encoders, an IMU, and a Velodyne lidar sensor. The testing area is mapped beforehand, and sensor readings are used to localize the wheelchair within the map. For control, the system publishes commanded twist values, which are translated to left and right wheel velocities and tracked by a low-level PID controller at 200 Hz.

## APPENDIX II DATASET CREATION AND VISUALIZATIONS

In this paper, we design an image processing pipeline to track the ball and the wheelchair in video footage. This section provides more details about the automatic dataset creation process and some of the issues detected.

### A. Details of Automatic Dataset Creation

The objective of this phase is to extract useful data on player movements during gameplay to create a dataset suitable for model training. We began with videos of nine wheelchair tennis singles matches from the Tokyo 2020 Paralympic Games. The process involved six stages: (1) training a neural network to identify ball hit audio segments, (2) training a mean-shift model to identify non-matchplay segments, (3) obtaining court homography, (4) locating the tennis ball, (5) locating the closest player, and (6) combining aggregated data for training output.

**Model for Matchplay Detection:** The video-based model uses a Mean Shift clustering algorithm to classify frames as either valid or invalid. Valid frames include a full overhead view of the tennis court, essential for collecting data on player movements and responses, while invalid frames show players recovering, commentators, detailed scoresheets, and crowd views. The model was trained on manually labeled video frames, preprocessed with resizing, Gaussian filtering, grayscale conversion, and intensity rescaling to enhance accuracy. The Mean Shift algorithm was applied to the feature vectors of the training data to learn the underlying clusters, identifying one cluster for valid frames and others for variations of invalid frames. The model achieved an accuracy of 99.62% and an F-score of 99.63% on the test dataset.

**Model for Hit Detection:** An audio-based model was trained to detect hits by identifying audio segments containing sounds resembling a player hitting the ball. Hit sounds

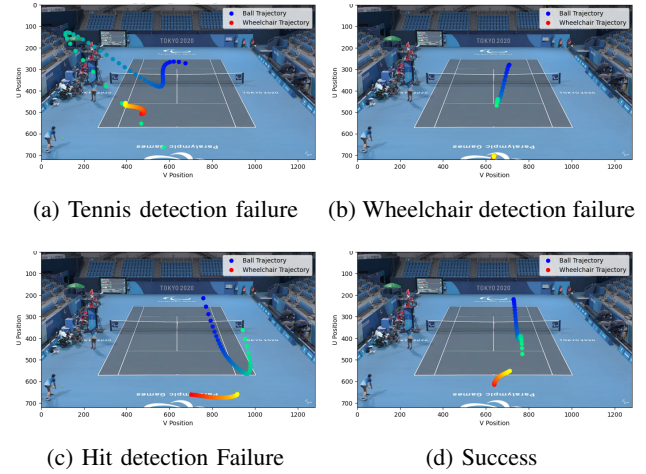


Fig. 10: Dataset visualizations: failure modes and success.

are distinctive, while other match sounds include commentary, ball bounces, and typical match noise. The model architecture is a sequential neural network with dense layers and dropout regularization, processing audio segments using mel-frequency cepstral coefficients (MFCCs), chromagrams, and mel-spectrograms to create a flattened feature vector.

For training, we manually labeled timestamps of player hits in a small segment of a match, isolated the corresponding audio clips for hits, and selected non-overlapping segments for non-hits. The model, trained with categorical cross-entropy loss, achieved an accuracy of 92.3%, effectively identifying timestamps for hits.

We initially used visual heuristics to detect changes in ball movement but found that audio extraction was more reliable due to unclear views and perspective distortion in broadcast videos. These visual challenges, particularly on the far side of the court, often led our algorithm to misinterpret the ball hitting the net as a successful return. As a result, generating accurate training data became difficult, and even TrackNet struggled to track the ball in such conditions consistently.

### B. Video Processing Visualization

Here, we visualize the success and failure modes of ball and wheelchair detection to better explain our experimental results. The failure modes mainly include ball detection failure, wheelchair detection failure, and hit detection failure, as shown in Figure 10.

From Figure 10a, we observe that the algorithm sometimes mistakenly identifies an object in the audience as the tennis ball, causing the trajectory to bend towards it. Figure 10b shows a failure in wheelchair detection where the algorithm misidentifies the Paralympics pattern as the wheelchair. Additionally, Figure 10c shows that the racket-ball hitting point is sometimes not well estimated, resulting in incorrectly cut trajectories that include part of the return. Conversely, Figure 10d demonstrates successful detection and tracking of the ball and wheelchair, as well as accurate hit detection, highlighting the pipeline’s potential effectiveness when operating correctly. Our policy achieves improved performance



when a human identifies and removes flawed or problematic trajectories from the training dataset.

### APPENDIX III IMITATION LEARNING MODEL PARAMETERS

In this section, we present the training parameters of the imitation learning models used in our study. The prediction horizon ( $L_p$ ) indicates the total number of waypoints that the model predicts for the path per inference. The history length ( $L_h$ ) is the number of the observed trajectory points based on which we are predicting the future. See Table III-VI for the hyperparameters we use for each imitation policy.

TABLE III: Diffusion

Parameter Name	Notation	Value
Learning rate	$l_d$	2e-5
Weight decay	$wd$	0
Prediction horizon	$L_p$	18
History length	$L_h$	32
Epoch number	$N_d$	1000

TABLE IV: ACT

Parameter Name	Notation	Value
Learning rate	$l_d$	1e-5
Weight decay	$wd$	0
Prediction horizon	$L_p$	18
History length	$L_h$	32
Epoch number	$N_d$	200

TABLE V: FCR

Parameter Name	Notation	Value
Learning rate	$l_d$	1e-3
Weight decay	$wd$	0
Prediction horizon	$L_p$	18
History length	$L_h$	32
Epoch number	$N_d$	1000

TABLE VI: AE-FCR

Parameter Name	Notation	Value
Learning rate	$l_d$	1e-3
Weight decay	$wd$	0.75
Prediction horizon	$L_p$	18
History length	$L_h$	32
Epoch number	$N_d$	500

### APPENDIX IV PHYSICAL ROBOT EXPERIMENT DETAILS

In this section, we introduce the details of our real-world experiments.

#### A. Vision System

To track and detect the tennis ball, we employ a multi-camera setup. The system consists of six Blackfly S cameras, each connected to a Jetson Xavier. The cameras are mounted on the back walls of the court at a height of 5.5 meters, looking down at the court. Three cameras are mounted on each side of the court, providing overlapping coverage of the entire court (Figure 11). This setup maximizes the chances of detecting the ball with multiple cameras and allows us to track the ball from various angles, making the system more robust than using cameras from the same angle. The Jetsons detect the ball in the images and share the detections over Ethernet to a central computer that computes the ball state (location and velocity) based on detections from different cameras. To estimate the dynamic states of the tennis ball—position, velocity, and spin—we utilize a factor graph that processes data asynchronously [56]. This approach aggregates the detection results from all six cameras asynchronously and publishes accurate estimation and prediction of the states. For real-time performance in inference, the GTSAM package [61], which is based on the ISAM2 algorithm [62], is employed. The inference and prediction speed in total is about 300 Hz, which is sufficient for our real time experiments.

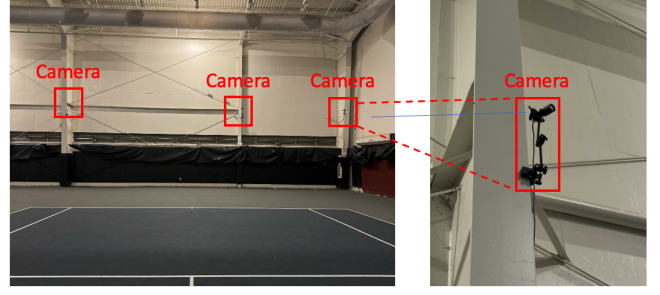


Fig. 11: Camera configurations in the real court: cameras are boxed and zoomed in.

#### B. Hybrid Testing Details

We conduct hardware-in-the-loop testing on a robotic wheelchair in an enclosed space, as shown in Figure 12. The real-world ball trajectories from the collected dataset are replayed one by one, and the robot acts according to the control architecture shown in Figure 13. Our control system runs on the ROS framework, with ROS nodes distributed across two computers: a high-performance workstation and an on-board PC (NUC). These computers communicate over WiFi, exchanging information through ROS topics. We run the imitation policy on the workstation due to its high computational requirements, which the on-board PC cannot handle. The imitation policy receives odometry information from the on-board PC and the ball trajectory converted to 2D image space, generating a local plan for the wheelchair. This local plan is then sent back to the on-board PC. The PD feedback controller on the on-board PC provides the command velocities based on the current odometry and the local plan. We record the wheelchair odometry data and the ball's 3D data, which can be post-processed to determine if the robotic wheelchair successfully intercepted the ball.

Figure 12 illustrates our imitation learning-based motion planner in action, combined with the real robot PD feedback control results. The top row shows the wheelchair in an enclosed space, while the bottom row displays the corresponding positions on the tennis court. The wheelchair starts from the center position of the baseline on the tennis court (shown in Figure 12a) and navigates to intercept the ball served to the right side of the court (Figures 12a-12e).

### APPENDIX V GENERALIZABILITY OF DATA EXTRACTION APPROACH

A contribution of our work is the development of an efficient, integrated pipeline that transforms raw broadcast tennis videos into data suitable for robot learning applications. To illustrate its effectiveness and flexibility, we adapted this pipeline to analyze table tennis gameplay. With minimal adjustments, we successfully repurposed our data extraction pipeline from broadcast tennis matches to table tennis. We were able to complete essential tasks, such as homography identification, player tracking, and ball tracking, much more quickly using broadcast footage from the recent Paris Olympics—a process that previously required extensive time and effort to optimize for tennis.

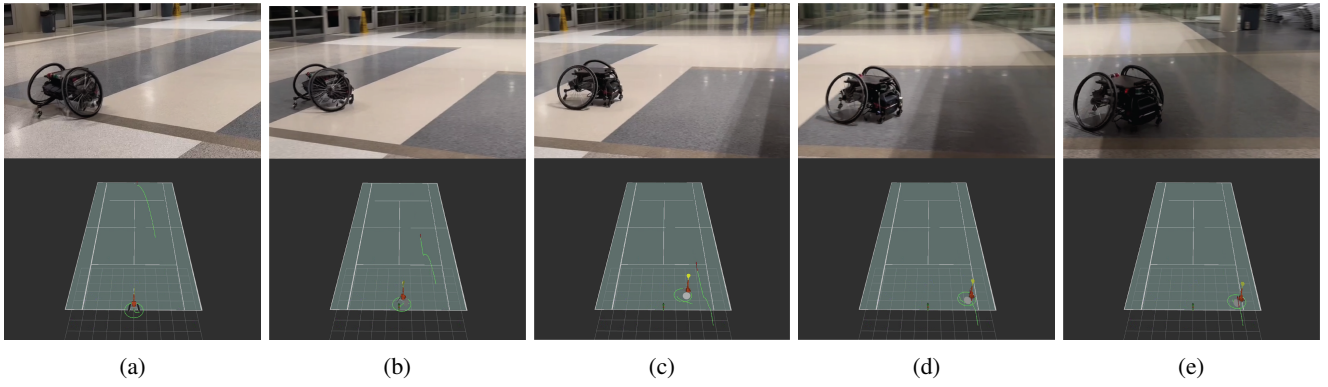


Fig. 12: We visualize the hardware-in-the-loop experiment on the robotic wheelchair. The ball is launched to the right side of the court, and the robotic wheelchair successfully navigates to intercept the ball.

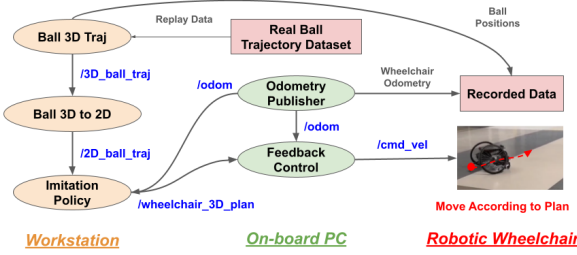


Fig. 13: Control architecture for hardware-in-loop testing.

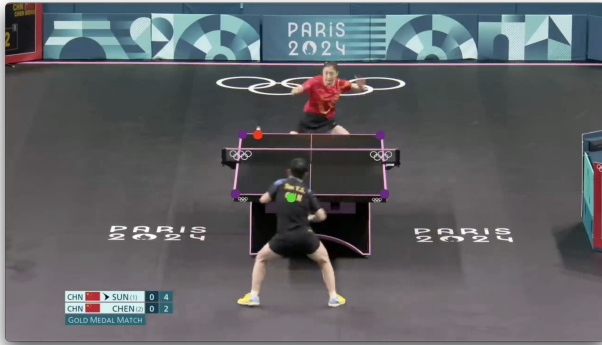


Fig. 14: Use the data collection pipeline for table tennis.

## REFERENCES

- [1] D. Büchler, S. Guist, R. Calandra, V. Berenz, B. Schölkopf, and J. Peters, "Learning to play table tennis from scratch using muscular robots," *IEEE Transactions on Robotics*, vol. 38, no. 6, pp. 3850–3860, 2022.
- [2] K. M. Lee, A. Krishna, Z. Zaidi, R. Paleja, L. Chen, E. Hedlund-Botti, M. Schrum, and M. Gombolay, "The effect of robot skill level and communication in rapid, proximate human-robot collaboration," in *Proceedings of the 2023 ACM/IEEE International Conference on Human-Robot Interaction*, ser. HRI '23. New York, NY, USA: Association for Computing Machinery, 2023, p. 261–270. [Online]. Available: <https://doi.org/10.1145/3568162.3577002>
- [3] D. B. D'Ambrosio, S. Abeyruwan, L. Graesser, A. Iscen, H. B. Amor, A. Bewley, B. J. Reed, K. Reymann, L. Takayama, Y. Tassa, et al., "Achieving human level competitive robot table tennis," *arXiv preprint arXiv:2408.03906*, 2024.
- [4] S. Mori, K. Tanaka, S. Nishikawa, R. Niiyama, and Y. Kuniyoshi, "High-speed humanoid robot arm for badminton using pneumatic-electric hybrid actuators," *IEEE Robotics and Automation Letters*, vol. 4, no. 4, pp. 3601–3608, 2019.
- [5] M. Liu, B. Depraetere, G. Pinte, I. Grondman, and R. Babuška, "Model-free and model-based time-optimal control of a badminton robot," in *2013 9th Asian Control Conference (ASCC)*, 2013, pp. 1–6.
- [6] Z. Zaidi, D. Martin, N. Belles, V. Zakharov, A. Krishna, K. M. Lee, P. Wagstaff, S. Naik, M. Sklar, S. Choi, Y. Kakehi, R. Patil, D. Mallemadugula, F. Pesce, P. Wilson, W. Hom, M. Diamond, B. Zhao, N. Moorman, R. Paleja, L. Chen, E. Seraj, and M. Gombolay, "Athletic mobile manipulator system for robotic wheelchair tennis," *IEEE Robotics and Automation Letters*, vol. 8, no. 4, pp. 2245–2252, 2023.
- [7] MRMC, "Bolt," 2024. [Online]. Available: <https://www.mrmoco.com/motion-control/bolt/>
- [8] F. Yang, Z. Shi, S. Ye, J. Qian, W. Wang, and D. Xuan, "Varsm: Versatile autonomous racquet sports machine," in *2022 ACM/IEEE 13th International Conference on Cyber-Physical Systems (ICCPs)*. IEEE, 2022, pp. 203–214.
- [9] A. Krishna, Z. Zaidi, L. Chen, R. Paleja, E. Seraj, and M. Gombolay, "Utilizing human feedback for primitive optimization in wheelchair tennis," *arXiv preprint arXiv:2212.14403*, 2022.
- [10] T. Haarnoja, B. Moran, G. Lever, S. H. Huang, D. Tirumala, J. Humpalik, M. Wulfmeier, S. Tunyasuvunakool, N. Y. Siegel, R. Hafner, et al., "Learning agile soccer skills for a bipedal robot with deep reinforcement learning," *Science Robotics*, vol. 9, no. 89, p. eadi8022, 2024.
- [11] J. Siegel and D. Morris, "Robotics, automation, and the future of sports," *21st Century Sports: How Technologies Will Change Sports in the Digital Age*, pp. 53–72, 2020.
- [12] A. Nakashima, D. Ito, and Y. Hayakawa, "An online trajectory planning of struck ball with spin by table tennis robot," in *2014 IEEE/ASME International Conference on Advanced Intelligent Mechatronics*. IEEE, 2014, pp. 865–870.
- [13] Z. Zhang, D. Xu, and M. Tan, "Visual measurement and prediction of ball trajectory for table tennis robot," *IEEE Transactions on Instrumentation and Measurement*, vol. 59, no. 12, pp. 3195–3205, 2010.
- [14] O. Koç, G. Maeda, and J. Peters, "A new trajectory generation framework in robotic table tennis," in *2016 IEEE/RSJ International Conference on Intelligent Robots and Systems (IROS)*. IEEE, 2016, pp. 3750–3756.
- [15] G. Zhang, C. Wang, B. Li, and H. Zheng, "Motion planning of a dual manipulator system for table tennis," in *Intelligent Autonomous Systems 12: Volume 2 Proceedings of the 12th International Conference IAS-12, held June 26-29, 2012, Jeju Island, Korea*. Springer, 2013, pp. 335–344.
- [16] D. Serra, A. C. Satici, F. Ruggiero, V. Lippiello, and B. Siciliano, "An optimal trajectory planner for a robotic batting task: the table tennis example," in *International Conference on Informatics in Control, Automation and Robotics*, vol. 3. SCITEPRESS, 2016, pp. 90–101.
- [17] K. Mülling, J. Kober, and J. Peters, "A biomimetic approach to robot table tennis," *Adaptive Behavior*, vol. 19, no. 5, pp. 359–376, 2011.
- [18] Y. Ji, X. Hu, Y. Chen, Y. Mao, G. Wang, Q. Li, and J. Zhang, "Model-based trajectory prediction and hitting velocity control for a new



- table tennis robot,” in *2021 IEEE/RSJ International Conference on Intelligent Robots and Systems (IROS)*. IEEE, 2021, pp. 2728–2734.
- [19] S. Josef and A. Degani, “Deep reinforcement learning for safe local planning of a ground vehicle in unknown rough terrain,” *IEEE Robotics and Automation Letters*, vol. 5, no. 4, pp. 6748–6755, 2020.
  - [20] C. Wen, X. Lin, J. So, K. Chen, Q. Dou, Y. Gao, and P. Abbeel, “Any-point trajectory modeling for policy learning,” *arXiv preprint arXiv:2401.00025*, 2023.
  - [21] W. Gao, L. Graesser, K. Choromanski, X. Song, N. Lazic, P. Sanketi, V. Sindhwani, and N. Jaitly, “Robotic table tennis with model-free reinforcement learning,” in *2020 IEEE/RSJ International Conference on Intelligent Robots and Systems (IROS)*. IEEE, 2020, pp. 5556–5563.
  - [22] S. W. Abeyruwan, L. Graesser, D. B. D’Ambrosio, A. Singh, A. Shankar, A. Bewley, D. Jain, K. M. Choromanski, and P. R. Sanketi, “i-sim2real: Reinforcement learning of robotic policies in tight human-robot interaction loops,” in *Conference on Robot Learning*. PMLR, 2023, pp. 212–224.
  - [23] C. Chi, S. Feng, Y. Du, Z. Xu, E. Cousineau, B. Burchfiel, and S. Song, “Diffusion policy: Visuomotor policy learning via action diffusion,” in *Proceedings of Robotics: Science and Systems (RSS)*, 2023.
  - [24] T. Z. Zhao, V. Kumar, S. Levine, and C. Finn, “Learning fine-grained bimanual manipulation with low-cost hardware,” *arXiv preprint arXiv:2304.13705*, 2023.
  - [25] S. Bahl, R. Mendonca, L. Chen, U. Jain, and D. Pathak, “Affordances from human videos as a versatile representation for robotics,” in *Proceedings of the IEEE/CVF Conference on Computer Vision and Pattern Recognition*, 2023, pp. 13 778–13 790.
  - [26] A. S. Chen, S. Nair, and C. Finn, “Learning generalizable robotic reward functions from ‘in-the-wild’ human videos,” *arXiv preprint arXiv:2103.16817*, 2021.
  - [27] H. Zhang, Y. Yuan, V. Makoviychuk, Y. Guo, S. Fidler, X. B. Peng, and K. Fatahalian, “Learning physically simulated tennis skills from broadcast videos,” *ACM Trans. Graph.*
  - [28] F. Torabi, G. Warnell, and P. Stone, “Behavioral cloning from observation,” *arXiv preprint arXiv:1805.01954*, 2018.
  - [29] M. Chang, A. Gupta, and S. Gupta, “Semantic visual navigation by watching youtube videos,” *Advances in Neural Information Processing Systems*, vol. 33, pp. 4283–4294, 2020.
  - [30] D. B. D’Ambrosio, J. Abelian, S. Abeyruwan, M. Ahn, A. Bewley, J. Boyd, K. Choromanski, O. Cortes, E. Coumans, T. Ding, *et al.*, “Robotic table tennis: A case study into a high speed learning system,” *arXiv preprint arXiv:2309.03315*, 2023.
  - [31] K. Dong, K. Pereida, F. Shkurti, and A. P. Schoellig, “Catch the ball: Accurate high-speed motions for mobile manipulators via inverse dynamics learning,” in *2020 IEEE/RSJ International Conference on Intelligent Robots and Systems (IROS)*. IEEE, 2020, pp. 6718–6725.
  - [32] F. Chaumette and S. Hutchinson, “Visual servo control. i. basic approaches,” *IEEE Robotics & Automation Magazine*, vol. 13, no. 4, pp. 82–90, 2006.
  - [33] —, “Visual servo control. ii. advanced approaches [tutorial],” *IEEE Robotics & Automation Magazine*, vol. 14, no. 1, pp. 109–118, 2007.
  - [34] J. Gu, S. Kirmani, P. Wohlhart, Y. Lu, M. G. Arenas, K. Rao, W. Yu, C. Fu, K. Gopalakrishnan, Z. Xu, *et al.*, “Rt-trajectory: Robotic task generalization via hindsight trajectory sketches,” *arXiv preprint arXiv:2311.01977*, 2023.
  - [35] Y. Mezouar and F. Chaumette, “Path planning for robust image-based control,” *IEEE transactions on robotics and automation*, vol. 18, no. 4, pp. 534–549, 2002.
  - [36] S. Feng, Z. Wu, Y. Zhao, and P. A. Vela, “Image-based trajectory tracking through unknown environments without absolute positioning,” *IEEE/ASME Transactions on Mechatronics*, vol. 27, no. 4, pp. 2098–2106, 2022.
  - [37] M. Keshmiri and W.-F. Xie, “Image-based visual servoing using an optimized trajectory planning technique,” *IEEE/ASME Transactions on Mechatronics*, vol. 22, no. 1, pp. 359–370, 2016.
  - [38] X. B. Peng, A. Kanazawa, J. Malik, P. Abbeel, and S. Levine, “SfV: Reinforcement learning of physical skills from videos,” *ACM Transactions On Graphics (TOG)*, vol. 37, no. 6, pp. 1–14, 2018.
  - [39] H. Xiong, Q. Li, Y.-C. Chen, H. Bharadhwaj, S. Sinha, and A. Garg, “Learning by watching: Physical imitation of manipulation skills from human videos,” in *2021 IEEE/RSJ International Conference on Intelligent Robots and Systems (IROS)*. IEEE, 2021, pp. 7827–7834.
  - [40] D. A. Pomerleau, “Alvin: An autonomous land vehicle in a neural network,” *Advances in neural information processing systems*, vol. 1, 1988.
  - [41] S. Ross and D. Bagnell, “Efficient reductions for imitation learning,” in *Proceedings of the thirteenth international conference on artificial intelligence and statistics*. JMLR Workshop and Conference Proceedings, 2010, pp. 661–668.
  - [42] S. Ross, G. Gordon, and D. Bagnell, “A reduction of imitation learning and structured prediction to no-regret online learning,” in *Proceedings of the fourteenth international conference on artificial intelligence and statistics*. JMLR Workshop and Conference Proceedings, 2011, pp. 627–635.
  - [43] J. Sohl-Dickstein, E. Weiss, N. Maheswaranathan, and S. Ganguli, “Deep unsupervised learning using nonequilibrium thermodynamics,” in *International conference on machine learning*. PMLR, 2015, pp. 2256–2265.
  - [44] J. Ho, A. Jain, and P. Abbeel, “Denoising diffusion probabilistic models,” *Advances in neural information processing systems*, vol. 33, pp. 6840–6851, 2020.
  - [45] E. Perez, F. Strub, H. De Vries, V. Dumoulin, and A. Courville, “Film: Visual reasoning with a general conditioning layer,” in *Proceedings of the AAAI conference on artificial intelligence*, vol. 32, no. 1, 2018.
  - [46] R. Rombach, A. Blattmann, D. Lorenz, P. Esser, and B. Ommer, “High-resolution image synthesis with latent diffusion models,” in *Proceedings of the IEEE/CVF conference on computer vision and pattern recognition*, 2022, pp. 10 684–10 695.
  - [47] M. Janner, Y. Du, J. Tenenbaum, and S. Levine, “Planning with diffusion for flexible behavior synthesis,” in *International Conference on Machine Learning*, 2022.
  - [48] Z. Wu, S. Ye, M. Natarajan, and M. C. Gombolay, “Diffusion-reinforcement learning hierarchical motion planning in adversarial multi-agent games,” 2024.
  - [49] S. Ye, M. Natarajan, Z. Wu, and M. C. Gombolay, “Diffusion models for multi-target adversarial tracking,” in *2023 International Symposium on Multi-Robot and Multi-Agent Systems (MRS)*, 2023, pp. 142–148.
  - [50] M. Müller, *Fundamentals of music processing: Audio, analysis, algorithms, applications*. Springer, 2015, vol. 5.
  - [51] Y.-C. Huang, I.-N. Liao, C.-H. Chen, T.-U. İk, and W.-C. Peng, “Tracknet: A deep learning network for tracking high-speed and tiny objects in sports applications,” in *2019 16th IEEE International Conference on Advanced Video and Signal Based Surveillance (AVSS)*. IEEE, 2019, pp. 1–8.
  - [52] M. Bataille, “tennis-tracking,” 2022. [Online]. Available: [https://github.com/MaximeBataille/tennis\\_tracking](https://github.com/MaximeBataille/tennis_tracking)
  - [53] S. Vinyes Mora, “Computer vision and machine learning for in-play tennis analysis: framework, algorithms and implementation,” Ph.D. dissertation, Imperial College London, 2019.
  - [54] A. Caspi, “Tennisproject,” <https://github.com/avivcaspi/TennisProject>, 2021.
  - [55] G. Jocher, A. Chaurasia, and J. Qiu, “Ultralytics YOLO,” Jan. 2023. [Online]. Available: <https://github.com/ultralytics/ultralytics>
  - [56] Q. Xiao, Z. Zaidi, and M. Gombolay, “Multi-camera asynchronous ball localization and trajectory prediction with factor graphs and human poses,” in *2024 IEEE International Conference on Robotics and Automation (ICRA)*, 2024, pp. 13 695–13 702.
  - [57] T. Moore and D. Stouch, “A generalized extended kalman filter implementation for the robot operating system,” in *Intelligent Autonomous Systems 13: Proceedings of the 13th International Conference IAS-13*. Springer, 2016, pp. 335–348.
  - [58] H. Chen, Y. Han, D. Misra, X. Li, K. Hu, D. Zou, M. Sugiyama, J. Wang, and B. Raj, “Slight corruption in pre-training data makes better diffusion models,” 2024. [Online]. Available: <https://arxiv.org/abs/2405.20494>
  - [59] C. Rösmann, F. Hoffmann, and T. Bertram, “Integrated online trajectory planning and optimization in distinctive topologies,” *Robotics and Autonomous Systems*, vol. 88, pp. 142–153, 2017.
  - [60] J. Song, C. Meng, and S. Ermon, “Denoising diffusion implicit models,” *arXiv preprint arXiv:2010.02502*, 2020.
  - [61] F. Dellaert and G. Contributors, “borglab/gtsam,” May 2022. [Online]. Available: <https://github.com/borglab/gtsam>
  - [62] M. Kaess, H. Johannsson, R. Roberts, V. Ila, J. J. Leonard, and F. Dellaert, “isam2: Incremental smoothing and mapping using the bayes tree,” *The International Journal of Robotics Research*, vol. 31, no. 2, pp. 216–235, 2012.